Evolution of Spur-Length Diversity in Aquilegia Petals Is Achieved Solely Through Cell-Shape Anisotropy

Evolution of spur length diversity in *Aquilegia* petals is achieved solely through cell shape anisotropy

Joshua R. Puzey,[1,*] Sharon J. Gerbode,[2,3,*] Scott A. Hodges,[4] Elena M. Kramer,[1,†] and L. Mahadevan[1,2]

[1] *Department of Organismic and Evolutionary Biology, Harvard University, Cambridge, MA 02138*
[2] *School of Engineering and Applied Sciences, Harvard University, Cambridge, MA 02138*
[3] *Wyss Institute for Biologically Inspired Engineering, Harvard University, Cambridge, MA 02138*
[4] *Department of Ecology, Evolution and Marine Biology, University of California, Santa Barbara, CA 93106*

The role of petal spurs and specialized pollinator interactions has been studied since Darwin. *Aquilegia* petal spurs exhibit striking size and shape diversity, correlated with specialized pollinators ranging from bees to hawkmoths in a textbook example of adaptive radiation. Despite the evolutionary significance of spur length, remarkably little is known about *Aquilegia* spur morphogenesis and its evolution. Utilizing experimental measurements, both at tissue and cellular levels, combined with numerical modeling, we have investigated the relative roles of cell divisions and cell shape in determining the morphology of the *Aquilegia* petal spur. Contrary to decades old hypotheses implicating a discrete meristematic zone as the driver of spur growth, we find that *Aquilegia* petal spurs develop via anisotropic cell expansion. Furthermore, changes in cell anisotropy account for 99% of the spur length variation in the genus, suggesting that the true evolutionary innovation underlying the rapid radiation of *Aquilegia* was the mechanism of tuning cell shape.

Keywords: petal shape, cell shape, evolution, pollination syndrome, morphogenesis, nectar spur

1. INTRODUCTION

Floral spurs are tubular pockets that grow out from developing floral organs (figure 1), typically with nectar-producing glands at their distal tip. Nectar spurs have evolved multiple times across the angiosperms often in association with dramatic speciation events, such as in the families Tropaeolaceae (Nasturtium), Fumariaceae (Bleeding-Heart), and Lentibulariaceae (Bladderwort) [1]. A particularly striking example of morphological diversity is seen in the genus *Aquilegia*, commonly known as columbine. Species of *Aquilegia* vary dramatically in spur length over a 16-fold range, matching the tongue lengths of their major pollinators, i.e., bees, hummingbirds and hawkmoths [2] (figure 1; electronic supplementary material; figures S1 and S2). The fit between the pollinator's tongue length and a species' spur length is apparently driven by selection acting to maximize pollen removal and receipt [2, 3], resulting in very rapid evolution of spur length at the time of speciation, and thereby contributing to the rapid radiation of the genus [2]. Despite their critical role in the ecology and diversification of *Aquilegia*, remarkably little is understood about spur morphogenesis and its evolution. Here we have used molecular, developmental and morphometric approaches to understand spur morphogenesis and the developmental basis of spur diversity in *Aquilegia*.

2. SPUR DEVELOPMENT: CONNECTING TISSUE MORPHOGENESIS WITH CELL SHAPE

Since Darwin [4], botanists have appreciated the evolutionary significance of petal spurs, yet spur development remains largely uncharacterized. In *Aquilegia*, traditional botanical hypotheses based on early histological studies hold that spur development is driven by meristematic knobs flanking the attachment point in the developing petal [5, 6]. In this

*These authors contributed equally to this work.
†Author for correspondence (ekramer@oeb.harvard.edu)

scenario, continued cell divisions combined with cell expansion are the primary driver of spur growth. Since Tepfer [5] the idea that spur growth occurs by essentially adding material one cell at a time has been widely accepted [6, 7] but has never been verified.

We experimentally tested this meristem hypothesis in *Aquilegia* by marking cell divisions with *in situ* hybridization [8] of *AqHistone4* (*AqHIS4*), which marks DNA-replicating cells, in developing petal spurs (figure 2, electronic supplementary material; section M1). This analysis revealed that while cell divisions are initially diffuse throughout the petal primordium, they cease early in development in a wave that begins at the distal petal tip and progresses toward the site of the initiating spur (figures 2*a-d*). Cell divisions are no longer visible anywhere in the young spur once it achieves a cup-like shape of size ∼5 mm (figure 2*d*). Furthermore, by directly counting the number of cells in a single cell file extending along the entire spur length, we determined that cell divisions completely cease early in development once the spur reaches a length of ∼5-9 mm (figure 2*e*, electronic supplementary material; section M2). Together, these results unequivocally demonstrate that spur growth is not driven by a meristematic zone. Thus, cell expansion, not cell division, must be the primary driver of spur outgrowth once the prepattern is established by localized cell division. However, isotropic cell expansion alone would simply result in a scaled-up version of the initial cup-like spur; clearly an additional mechanism is needed to achieve the observed slender, elongated morphology (figure 1, electronic supplementary material; figures S1 and S2).

To investigate if and how cellular mechanisms are responsible for spur sculpting, we measured cell size and shape along a continuous transect of the outer (abaxial) epidermis in developing *A. coerulea* 'Origami' red/white spurs (hereafter referred to as *A. coerulea*) at 11 developmental stages following the cessation of cell division and until spur maturity (figure 3*a,b*). Since cells are consistently oriented along the long axis of the spur, we defined and measured cell length $l(s)$ and cell width $w(s)$ at a distance s (in mm) from the nectary tip, for a total of ∼7000 cell measurements (figure 3*b*, electronic supplementary material; figure S4 and sections M3 and M4). Given that petal lamina thickness is virtually uniform throughout the spur (electronic supplementary material; figure S4), cell size can be characterized by cell area $A(s) = lw$, while cell shape is characterized by the anisotropy defined as $\epsilon(s) = l/w$ along the spur. We see that although cell area increases uniformly along the entire spur during development (electronic supplementary material; figure S5), cell anisotropy varies along the length of the spur (figure 3*b,c*). To characterize the temporal development of the spur, we scaled the distance s by the instantaneous length of the spur L, a measure of developmental time, so that the scaled distance $z = s/L$ varies from $z = 0$ at the nectary tip to $z = 1$ at the attachment point (figure 3*a*) at each developmental stage. This allowed us to compare cell anisotropy $\epsilon(z)$ through development (figure 3*c*) and shows that although young spurs start out with $\epsilon(z) \approx 1$ (cells are approximately isotropic), as development progresses $\epsilon(z)$ increases non-uniformly along the length of the spur, reaching a maximum value just above the nectary. In figure 3*d*, the maximum cell anisotropy ϵ_{max} is plotted against the spur length L and demonstrates that spur development is associated with increasing cell anisotropy.

In addition to cell morphology measurements during development, we also recorded the shape of the entire spur at each stage. While cell columns along the length of the spur twist slightly during growth (electronic supplementary

material; figure S6), spur shape remains cylindrically symmetric throughout development, but becomes increasingly slender and elongated. Thus spur shape can be quantified by measuring its radial profile $r(s)$ (figure 3; electronic supplementary material; figures S7-S9, electronic supplementary material; section M5). To correlate cell morphology changes during development with the observed shape of the spur, we started with an 'initial' spur shape obtained by averaging radial profiles of two young (∼8 mm) *A. coerulea* spurs. This model spur profile was then numerically 'grown' utilizing experimental measurements of cell area $A(s)$ and cell anisotropy $\epsilon(s)$ to achieve spur profiles at the same developmental stages shown in figure 3*a*. The profiles were then rotated about the long axis of the spur to generate spur shapes at each developmental stage. The good agreement between the numerical and experimental spur profiles and shapes (figure 3*e,f*), with no adjustable parameters, demonstrates the critical role of cell shape in spur morphogenesis and directly connects measured cellular level data with organ level morphology. This is further confirmed by comparing the profiles calculated using only cell area changes while ignoring cell anisotropy, which result in deformed, short wide spurs (electronic supplementary material; figure S10 and section M6).

Having linked changes in cell anisotropy to the sculpting of spur morphology, we sought to experimentally perturb cell shape. In plant cells the cytoskeleton constrains the direction of cell elongation by orienting cellulose deposition [9]. Since disruption of the cytoskeleton should perturb cell anisotropy and therefore spur morphosis, we treated developing *A. chrysantha* spurs with oryzalin, a microtubule depolymerization agent [10, 11] (details in electronic supplementary material; figure S11 and section M7). As shown in figure 4, the treated spur is much shorter and wider than untreated spurs from the same flower. Examination of cells in the treated tissue verified that changes in cell area A are unaffected, while cell anisotropy remains at $\epsilon \approx 1$ (figure 4*b,c*) for all time points. These findings further confirm that anisotropic cell expansion, not extended meristematic growth, determines spur morphogenesis.

3. CELL ANISOTROPY AND SPUR LENGTH DIVERSITY

The essential role of cell anisotropy in *A. coerulea* spur morphogenesis raised the question of how variations in this parameter contribute to evolutionarily significant diversification of spur shape and length. Since mature petal spurs in *Aquilegia* range in length from $L \approx$ 1-15 cm, with the majority in the 2-6 cm range [2, 12], four *Aquilegia* species were studied to sample this entire range: *A. vulgaris* (final spur length $L_f \approx 2.4$ cm), *A. canadensis* ($L_f \approx 2.6$ cm), *A. coerulea* ($L_f \approx 5.1$ cm), and *A. longissima* ($L_f \approx 15.9$ cm) (figures 1 and 5*a*). These species also represent a breadth of associated pollinators from bee (short, curled spurs in *A. vulgaris*) to hummingbird (short straight spurs in *A. canadensis*) to hawkmoth (long slender spurs in *A. coerulea* and *A. longissima*). For each species, cellular measurements from 2-4 biological replicates were imaged at multiple developmental stages, using ESEM at three equally spaced locations along the axis of the spur and one point on the petal blade, for a total of ∼6500 independent cellular measurements (electronic supplementary material; figures S12 and S13 and section M8).

There are three possible contributors to the diversity in *Aquilegia* spur length: variation in cell number, cell size, or cell anisotropy. We have addressed the issue of cell number in two independent ways. First, as described above, we have demonstrated that all cell divisions cease in *A. vulgaris* petals by ∼ 5 mm. At this stage, spurs from the

other study species are indistinguishable, as are their cell size and shape, implying that cell number should not vary considerably between species. To verify this, we have also directly counted the number of cells in mature spurs from *A. canadensis*, *A. coerulea*, and *A. longissima* flowers (figure 2*e*). We find that the number of cells in each species varies by less than $30\% \pm 21\%$, whereas spur length varies by up to 600% (electronic supplementary material; section M2).

Having eliminated cell number as the primary contributor to spur length diversity, we expect to find that changes in cell size and/or cell anisotropy will be correlated with relative increase in spur length for each species. In figure 5*b*, we show that the relative increase in cell area, A_f/A_i (final cell area at spur maturity/cell area at the initial stage) is uncorrelated with the ratio of final to initial spur length, L_f/L_i. Here, the initial spur length L_i is the length of the spur once cell divisions have ceased, about 7 ± 2 mm (figure 2*e*). However, the relative increase in cell anisotropy, ϵ_f/ϵ_i, is strongly correlated with the ratio of final to initial spur length (figure 5*c*). The R^2 value of 0.99 indicates that variations in cell anisotropy account for 99% of the observed variation in mature spur length. Furthermore, each of the species follows the same growth curve (figure 5*d*), where total petal length, L_p, including the blade, is reported because spur length measurements in attached young petals are obstructed by sepals. Thus, length differences between these species are achieved through variations in the duration of cell elongation. For example, the developmental duration of the shortest spur studied, *A. vulgaris*, is ∼10 days, while in the longest spur studied, *A. longissima*, this duration is ∼16 days, so that longer periods of cell elongation lead to higher cell anisotropy, and consequently longer petal spurs.

4. DISCUSSION

We have shown that the *Aquilegia* petal spur is initially formed by a short period of localized cell divisions followed by an extended process of oriented cell elongation. Furthermore, diversity in spur length is mediated by variation in the degree of anisotropic cell elongation rather than the number or size of cells. The tight correlation of cell anisotropy with spur length suggests that even the extreme outlier *A. longissima* can reach its extraordinary spur length simply by increasing a single developmental parameter. Thus, minimal elaboration of an existing developmental mechanism can rapidly generate spur length variation in the genus in concert with a specific ecological pressure, the presence of a pollinator with a dramatically longer tongue. Interestingly, there are taxa within the genera *Semiaquilegia* and *Urophysa*, which are very closely related to *Aquilegia*, that lack elongated spurs but produce small nectary cups or extremely short spurs [6, 14, 15], similar to very early developmental stages in *Aquilegia*. This implies that the evolutionary innovation underlying spur formation and the rapid radiation of *Aquilegia* may have been the mechanism of tuning cell anisotropy, which led to the elaboration of of the nectary cup.

It is useful to consider the sculpting observed in *Aquilegia* spurs in a broader context of tissue elongation, which is at the heart of organ morphogenesis. Tissue elongation without cell division can occur via a combination of two mechanisms: convergent extension driven by cell migration in animals [16], or changes in cell shape anisotropy in instances where cells are immobile, such as in plants [17]. In tissues with active cell division, oriented divisions followed by isotropic cell expansion can also result in tissue elongation. Since any of these microscopic reorganizations

would lead to indistinguishable macroscopic deformations, all of these possibilities must be considered in phenotypic analysis of tissue morphogenesis [17, 18]. In the context of plant morphodynamics [19], our study has emphasized that in addition to differential cell division and isotropic cell expansion, differential cell anisotropy can also play a dominant role in evolutionarily significant shape change. Petal spur sculpting and spur length diversity across the genus *Aquilegia*, even in its most extreme expressions, can be explained solely through variation in cell anisotropy. Developmental perturbations using oryzalin have further demonstrated that changes in cell anisotropy are dependent on cytoskeletal arrangement. We know from work done in model plants that several major hormone pathways, as well as perturbations of the cytoskeleton itself, can influence oriented cell elongation [10, 20, 21]. Contrary to what has been suggested in the Lamiales [13], our developmental measurements imply that the duration of cell elongation plays a critical role in determining spur length. Genes underlying both hormone pathways that influence cell anisotropy and developmental duration should be explored as candidates for the control of spur development in *Aquilegia* as well as for the genetic basis of new pollinator syndromes that are associated with speciation of the genus. Diversification in association with pollinators is often associated with correlated shape variation in floral organs such as stamens, styles, corolla tubes, petals, and sepals [1, 22, 23], and begs the question of whether tuning cell anisotropy is exploited in other systems that exhibit evolutionarily significant morphological diversity.

We thank J. Dumais and T. Tallinen for helpful discussions, K. Haggerty and H. Puzey for assistance with image analysis, and members of the Kramer and Hodges lab groups for comments on the manuscript. This research was supported by funding from the MacArthur Foundation, the Wyss Institute, the Kavli Institute, Harvard NSF-MRSEC, NSF award IOS 0720240 (to E.M.K.), and NSF award EF-0412727 (to E.M.K. and S.A.H.).

[1] Hodges, S. A. & Arnold, M. L. 1995 Spurring plant diversification: Are floral nectar spurs a key innovation? *Philos. Trans. R. Soc. London Ser. B* **262**, 343.

[2] Whittall, J. B. & Hodges, S. A. 2007 Pollinator shifts drive increasingly long nectar spurs in columbine flowers. *Nature* **447**, 706. (DOI:10.1038/Nature05857)

[3] Fulton, M., & Hodges, S. A. 1999 Floral isolation between *Aquilegia formosa* and *Aquilegia pubescens*. *Proc. Roy. Soc. B* 266, 2247-2252.

[4] Darwin, C. 1885 *The Various Contrivances by Which Orchids are Fertilized by Insects*, 2nd edn. London:John Murray.

[5] Tepfer, S. S. 1953 Floral anatomy and ontogeny in *Aquilegia formosa* var. *truncata*, and *Ranunculus repens*. *Univ. Cal. Pub. Bot* **25**, 513-648.

[6] Tucker, S. C. & Hodges, S. A. 2005 Floral ontogeny of *Aquilegia*, *Semiaquilegia*, and *Enemion* (Ranunculaceae). *Int. J. Plant Sci.* **166**, 557-574.

[7] Erbar, C., Kusma, S., & Leins, P. 1999 Development and interpretation of nectary organs in Ranunculaceae. *Flora* **194**, 317-332.

[8] Kramer, E. M. 2005 Methods for studying the evolution of plant reproductive structures: comparative gene expression techniques. In *Molecular Evolution: Producing the Biochemical Data*, vol. 395 of *Methods in Enzymology*, pp. 617-636 San

Diego:Academic Press. (DOI: 10.1016/S0076-6879(05)95032-5)

[9] Baskin, T. I. 2005 Anisotropic expansion of the plant cell wall. *Annu. Rev. Cell Dev. Bio.* **21**, 203-222. (DOI: 10.1146/Annurev.Cellbio.20.082503.103053)

[10] Hamant, O. et al. 2008 Developmental patterning by mechanical signals in *Arabidopsis*. *Science* **322**, 1650-1655.

[11] Baskin, T. I., Wilson, J. E., Cork, A., & Williamson, R. E. 1994 Morphology and microtubule organization in *Arabidopsis* roots exposed to oryzalin or taxol. *Plant Cell Physiol.* **35**, 935-942.

[12] Munz, P. A. 1946 *Aquilegia*: the cultivated and wild columbines. *Gentes Herbarum* **7**, 150.

[13] Box, M. S., Dodsworth, S., Rudall, P. J., Bateman, R. M., & Glover, B. J. 2011 Characterization of Linaria KNOX genes suggests a role in petal-spur development. *Plant J.* (DOI: 10.1111/j.1365-313X.2011.04721.x)

[14] Wang, W. & Chen, Z.-D. 2007 Generic level phylogeny of Thalictroideae (Ranunculaceae) - implications for the taxonomic status of Paropyrum and petal evolution. *Taxon* **56**, 811-821.

[15] Wang, W., Lu, A.-M., Ren, Y., Endress, M. E., & Chen, Z.-D. 2009 Phylogeny and classification of Ranunculales: Evidence from four molecular loci and morphological data. *Perspect. Plant Ecol.* **11**, 81-110. (DOI: 10.1016/j.ppees.2009.01.001)

[16] Keller, R., Davidson, L., Edlund, A., Elul, T., Ezin, M., Shook, D., & Skoglund, P. 2000 Mechanisms of convergence and extension by cell intercalation. *Philos. Trans. R. Soc. London Ser. B* **355**, 897-922.

[17] Coen, E., Rolland-Lagan, A. G., Matthews, M., Bangham, J. A., & Prusinkiewicz, P. 2004 The genetics of geometry. *Proc. Natl Acad. Sci. USA* **101**, 4728-4735.

[18] Blanchard, G. B., Kabla, A. J., Schultz, N. L., Butler, L. C., Sanson, B., Gorfinkiel, N., Mahadevan, L., & Adams, R. J. 2009 Tissue tectonics: morphogenetic strain rates, cell shape change and intercalation. *Nature Methods* **6**, 458-U86.

[19] Chickarmane, V., Roeder, A. H. K., Tarr, P. T., Cunha, A., Tobin, C., & Meyerowitz, E. M. 2010 Computational morphodynamics: A modeling framework to understand plant growth., *Ann. Rev. Plant Bio.* **61**, 65-87.

[20] Lee, Y. K., Kim, G.-T., Park, J., Kwak, S.-S., Choi, G., & Chung, W.-I. 2006 *LONGIFOLIA1* and *LONGIFOLIA2*, two homologous genes, regulate longitudinal cell elongation in *Arabidopsis*. *Development* **133**, 4305-4314.

[21] Kim, G. T., Shoda, K., Tsuge, T., Cho, K. H., Uchimiya, H., Yokoyama, R., Nishitani, K., & Tsukaya, H. 2002 The *ANGUSTIFOLIA* gene of *Arabidopsis*, a plant *CtBP* gene, regulates leaf-cell expansion, the arrangement of cortical microtubules in leaf cells and expression of a gene involved in cell-wall formation. *EMBO* **21**, 1267-1279.

[22] Venail, J., Dell'Olivo, A., & Kuhlemeier, C. 2010 Speciation genes in the genus *Petunia*. *Philos. Trans. R. Soc. London Ser. B* **365**, 461-468.

[23] Bradshaw, H. D., Otto, K. G., Frewen, B. E., McKay, J. K., & Schemske, D. W. 1998 Quantitative trait loci affecting differences in floral morphology between two species of monkeyflower (Mimulus) *Genetics* **149**, 367-382.

FIG. 1: ***Aquilegia* flowers exhibit considerable spur length diversity.** All scale bars equal 1 cm. (*a*) *A. vulgaris*. (*b*) *A. canadensis*. (*c*) *A. coerulea*. (*d*) *A. longissima*.

FIG. 2: **Cell divisions cease very early in spur development.** (*a-d*) *In situ* localization of *AqHIS4* in developing *A. vulgaris* flowers was used to determine the pattern and extent of cell divisions in early petal development. *AqHIS4* expression, visualized by purple staining, marks cell divisions. Arrowheads, petals; Arrow, initiating spur. (*a*) Two young *A. vulgaris* flower buds (in brackets) showing ubiquitous *AqHIS4* expression indicating diffuse cell divisions. Scale bar equals 0.5 mm. (*b*) Older flower showing ubiquitous cell divisions in the petal while cell divisions have ceased in the stamens (St). Scale bar equals 0.5 mm. (*c*) *A. vulgaris* petal with initiating spur. Cell divisions are most concentrated at the initiating spur and have ceased in the tip of the developing petal as indicated by a dotted line. Scale bar equals 1 mm. (*d*) *A. vulgaris* spur of length $L \approx 5$ mm with no *AqHIS4* expression evident, indicating all cell divisions have ceased. Scale bar equals 1 mm. (*e*) The number of cells in a single cell file extending the entire length of developing *A. canadensis*, *A. coerulea*, and *A. longissima* spurs, counted from the attachment point to the nectary. The number of cells plateaus to a constant value early in development when the spur is ∼5-9 mm long. Errorbars indicate counting errors.

FIG. 3: **Cell anisotropy drives *A. coerulea* petal spur development.** (*a*) Developmental series of *A. coerulea* petals. Scale bar equals 1 cm. Both cellular measurements and spur radius r are recorded at the position s as measured from the nectary tip along the length of the spur. To compare between developmental stages, the position along the spur is also measured by z, which increases from 0 at the nectary to 1 at the attachment point. (*b*) Light microscope images are analyzed to determine cell anisotropy $\epsilon = l/w$ and cell area $A = lw$ at the position z along the spur. (*c*) Waterfall plot of ϵ versus z at different developmental stages measured by the spur length L. (*d*) The maximum cell anisotropy ϵ_{max} is highly correlated with spur length L. (*e*) Using measurements of cell anisotropy and cell area, in concert with an initial spur determined by averaging experimental spur profiles, numerically calculated spur shapes are generated without any free parameters at the same developmental stages shown in panel (*a*). Numerical spurs are shaded according to local cell anisotropy. (*f*) Numerically calculated spur profiles (circles) are overlaid on experimentally measured spur profiles (solid curves).

FIG. 4: **Cytoskeleton perturbations decouple isotropic cell expansion from cell anisotropy.** (*a*) Oryzalin (Oz), a microtubule depolymerization agent, was applied to the entire surface of single *Aquilegia* spurs after they had achieved into a short tubular shape of length $L \approx 1$ cm (right). Untreated petal from the same flower is shown as a control (left). Photos of petals were taken ∼6 days after initial application of oryzalin. Scale bar equals 1 cm. (*b*) Left: Anisotropically shaped cells from untreated spur. Right: Image of oryzalin treated spur showing isotropically shaped cells. (*c*) Comparison of cell area A and anisotropy ϵ between cells from oryzalin treated spurs (N = 270) and from untreated samples (N = 127).

FIG. 5: **Cell anisotropy plays an essential role in spur length diversity.** (*a*) Petals from four different *Aquilegia* species. From left to right: *A. longissima*, *A. coerulea*, *A. canadensis*, and *A. vulgaris*. Scale bar equals 1 cm. Insets for each species show a cellular region of identical width ∼30 μm. (*b*) The ratio of final to initial spur length L_f/L_i versus the fractional increase in cell area A_f/A_i is plotted to show that changes in spur length are not correlated with changes in cell area ($R^2 = 0.233$, Pearson's $r = -0.482$). (*c*) L_f/L_i is plotted versus the fractional increase in cell anisotropy ϵ_f/ϵ_i, measured at $z \approx 1/3$, indicating that spur length diversity is characterized by cell anisotropy ($R^2 = 0.990$, Pearson's $r = 0.995$). (*d*) Total petal length L_p is plotted versus time, demonstrating that all species follow the same growth curve but differ in developmental duration. Vertical errorbars indicate range in initial spur length L_i and horizontal errorbars in (*b*),(*c*) are comparable to marker size.

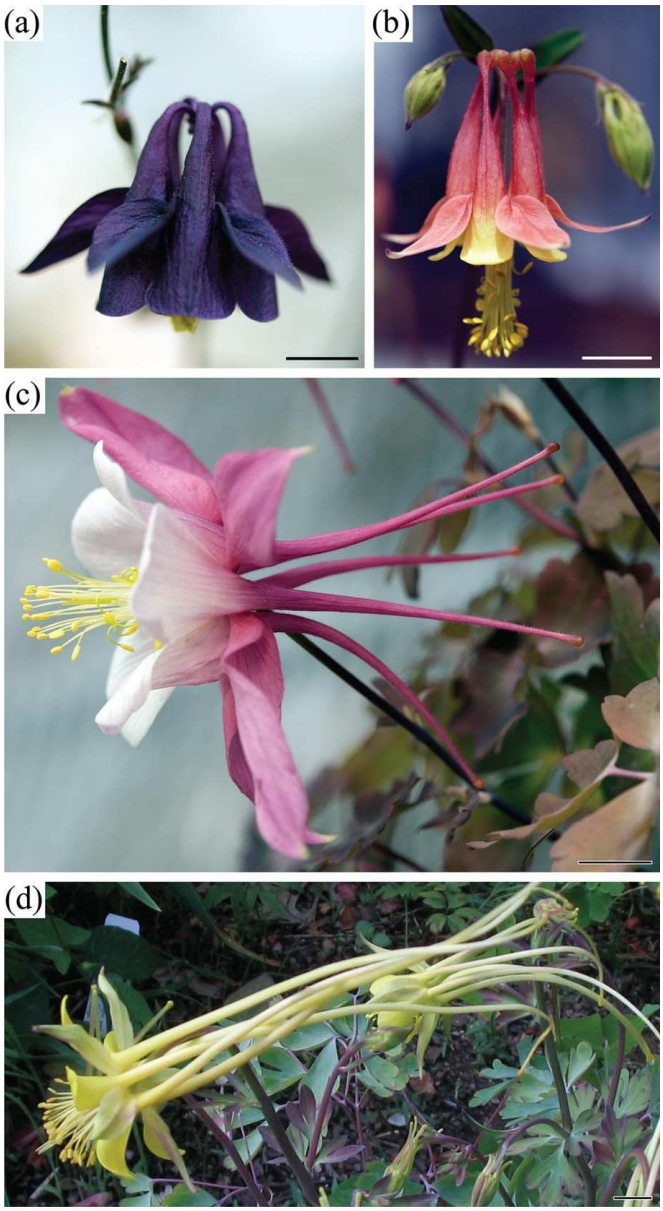

Figure 1
77x140mm (300 x 300 DPI)

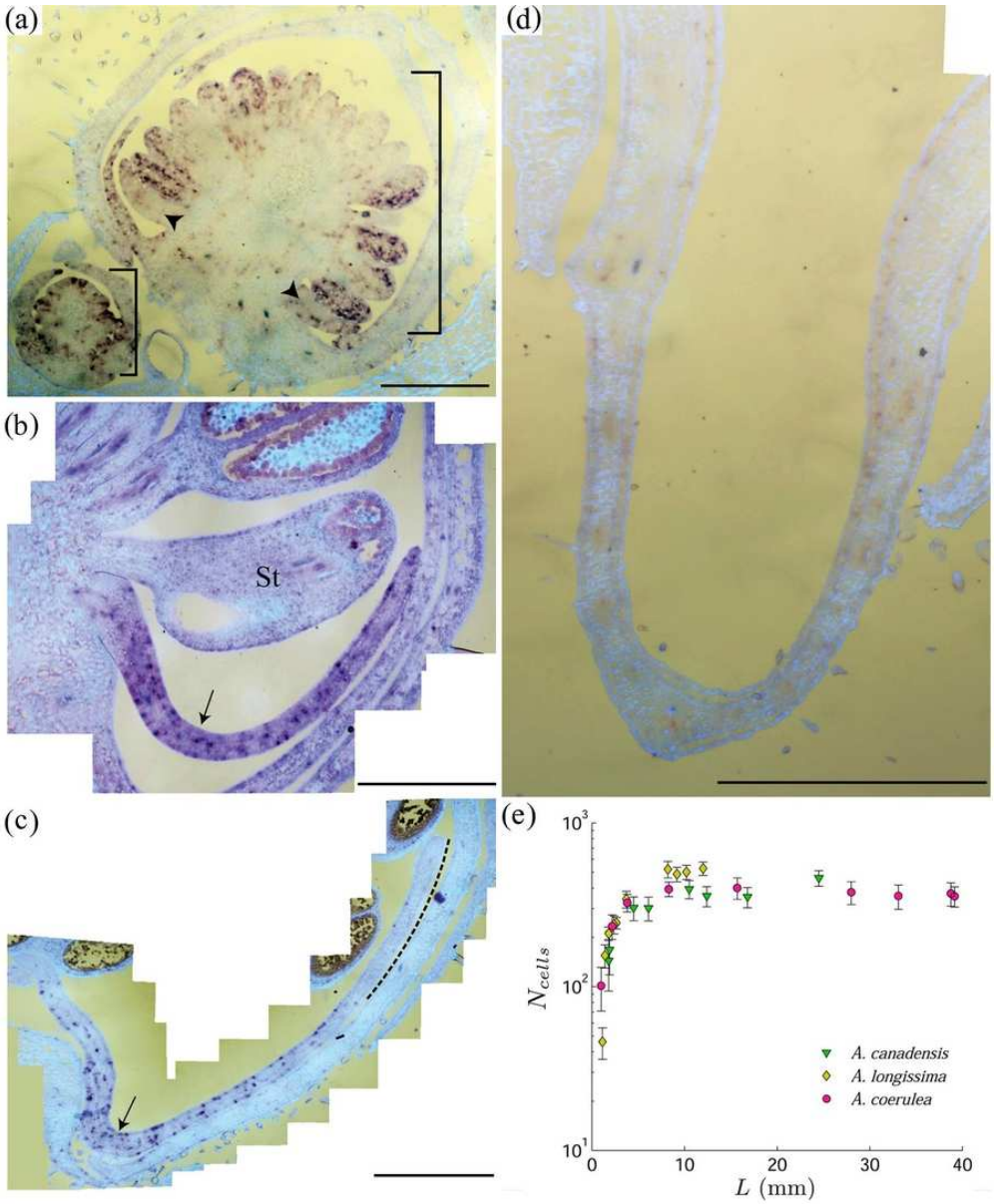

Figure 2
76x91mm (300 x 300 DPI)

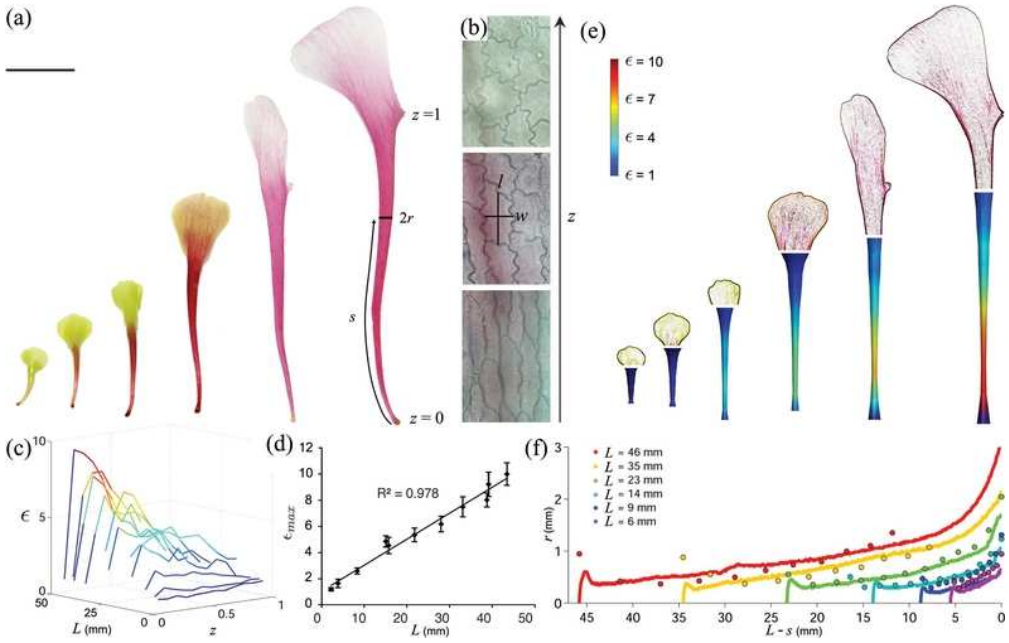

Figure 3
67x42mm (300 x 300 DPI)

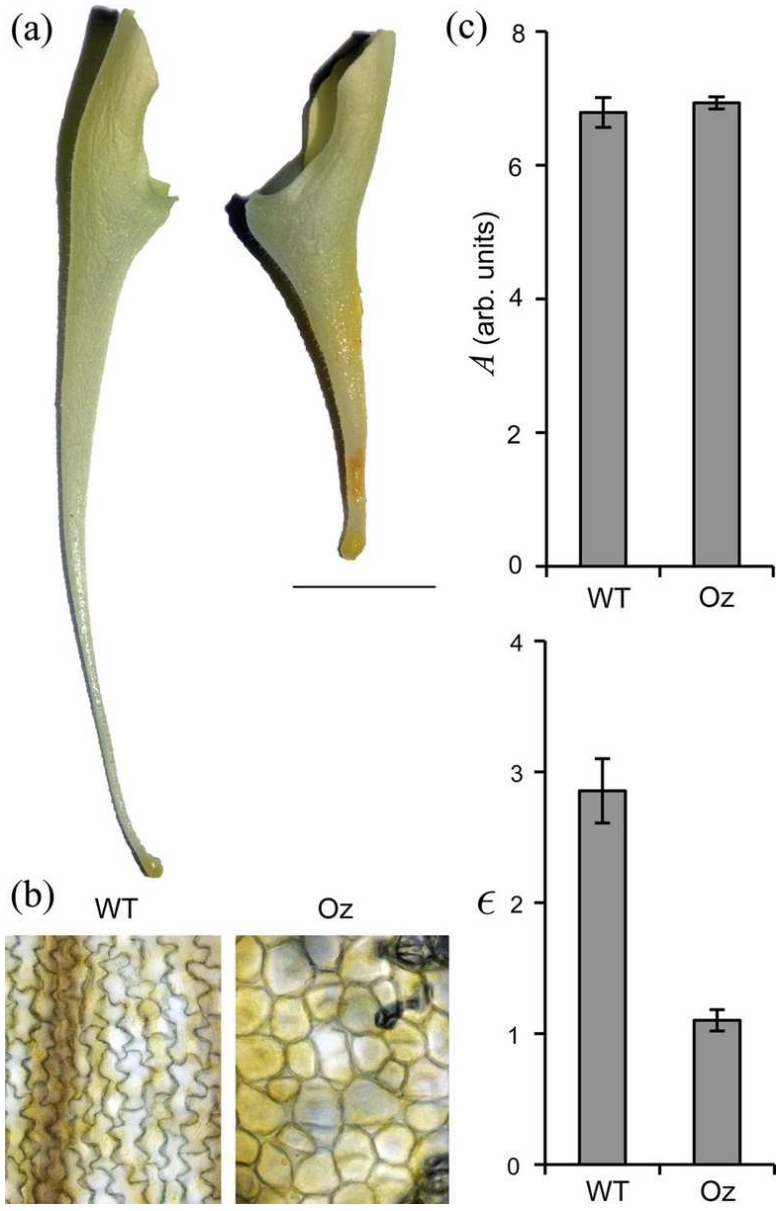

Figure 4
65x102mm (300 x 300 DPI)

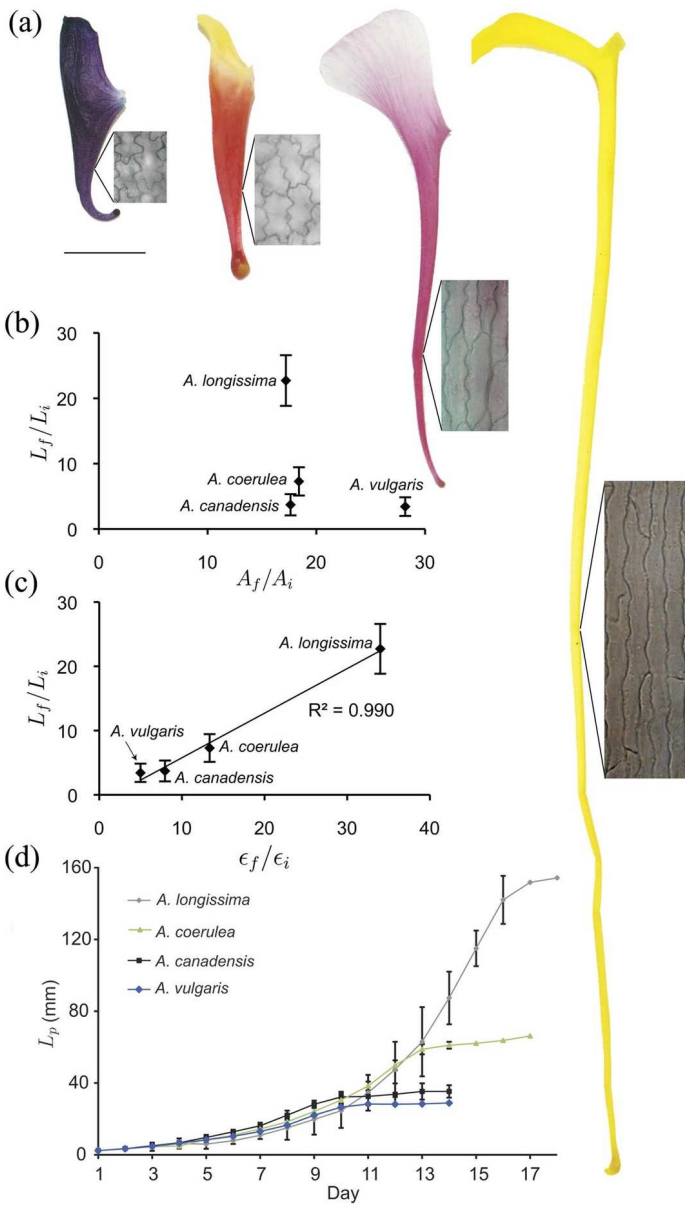

Figure 5
89x157mm (300 x 300 DPI)

Evolution of spur length diversity in *Aquilegia* petals is achieved solely through cell shape anisotropy: Electronic supplementary material

Joshua R. Puzey,[1,*] Sharon J. Gerbode,[2,3,*] Scott A. Hodges,[4] Elena M. Kramer,[1,†] and L. Mahadevan[1,2]

[1] *Department of Organismic and Evolutionary Biology, Harvard University, Cambridge, MA 02138*
[2] *School of Engineering and Applied Sciences, Harvard University, Cambridge, MA 02138*
[3] *Wyss Institute for Biologically Inspired Engineering, Harvard University, Cambridge, MA 02138*
[4] *Department of Ecology, Evolution and Marine Biology, University of California, Santa Barbara, CA 93106*

M1. CELL DIVISION MEASUREMENTS: *AqHistone4 in situ* METHODS

All plants for *in situ* hybridization and cell morphology studies were grown in environmentally controlled growth chambers and greenhouses at Harvard University at approximately 20 C with long-day conditions of 16hr light/8 hr dark. Seeds of *A. coerulea* Origami red/white were obtained from Swallowtail Seeds (Santa Rosa, CA).

AqHistone4 (*AqHIS4*) *in situ* hybridization was performed as described in [9]. *AqHIS4* marks DNA-replicating cells. Inflorescences for *in situ* hybridization were collected from *A. vulgaris*, fixed under vacuum in FAA, dehydrated, and embedded in Paraplast. For *in situ* probe preparation, *AqHIS4* was PCR amplified from cDNA using *AqHIS4*F 5'- AAGGCGTGGTGGTGTTAAGCGTATCA and *AqHIS4*R 5'- GAATTACAAGAAAGTAGTAGATCAGAATC-CAAC. Amplified fragments were cloned using TOPO-TA (Invitrogen) and digoxigenin-labeled RNA probes were synthesized from linearized plasmids. *AqHIS4* hybridized sections were stained with calcofluor and imaged with white and fluorescent light. Imaging was performed on a Leitz DMRD microscope using a Retiga EXi camera (Harvard Imaging Center).

M2. CELL COUNTING METHODS

The continuous scanning technique described in supplementary section M3 was used to generate 27 composite images for *A. canadensis*, *A. coerulea*, and *A. longissima* spurs at various developmental stages. For each composite spur image cells were counted manually starting at the attachment point and continuing to the nectary. Generating continuous cellular resolution images for *A. vulgaris* was not possible due to thick cuticular waxes. Composite scans of *A. longissima* spurs greater than 15 mm were not possible because the narrow spur radius prevented a deep focusing depth while maintaining cell focus and cutting and flattening the spur resulted in crushed cells. Counting errors, typically of about 40 cells, arose due to several factors: (1) uncertainty in the precise position of the attachment point, (2) zones of imperfect image quality, and (3) inherent error due to counting statistics.

The variation in number of cells at spur maturity was measured for *A. canadensis*, *A. coerulea*, *A. longissima*. The mean number of cells for spurs greater than $\sim$ 8 mm long was calculated for each species, and the counting error in this mean was estimated as described above. Taking the mean number of cells in mature *A. canadensis* as a

---

*These authors contributed equally to this work.
†Author for correspondence (ekramer@oeb.harvard.edu)

reference point, we calculated the fractional variation from this value in *A. coerulea* and *A. longissima*. This process showed that there are $4\% \pm 24\%$ fewer cells in *A. coerulea* than *A. canadensis*, and there are $30\% \pm 21\%$ more cells in *A. longissima* than *A. canadensis*, where the errors in these values were propagated from the error in the number of cells for each species.

M3. LIGHT MICROSCOPE METHODS

For continuous *A. coerulea* 'Origami' red/white (hereafter referred to as *A. coerulea*) cellular data shown in Fig. 3, spurs were imaged using Zeiss AxioCam Mrc digital camera mounted on a Zeiss AxioImager.Z2 microscope (Harvard Imaging Center). Petals were cut longitudinally through the attachment point and nectary, mounted on glass slide with a thin layer of fingernail polish and imaged immediately in order to prevent any drying and distortion of cells. This allowed for direct microscope imaging of the cells of the outer (abaxial) epidermis. Since *Aquilegia* petal spurs remain only about 3 cell layers thick during all stages of development, the morphological trends observed in the epidermis are a good indicator of cell behavior throughout the thickness of the spur. Moreover, the *in situ* studies indicated that cell divisions ceased throughout all layers of the spurs at the same time, suggesting that cell expansion must be responsible for spur elongation across all cell layers. Overlapping images were taken at the same magnification along the entire length of the spur. Individual images were stitched together using Adobe Photoshop CS3, creating a composite image (Fig. SS4).

M4. CELL AND SPUR MORPHOLOGY MEASUREMENTS

(a) Cell anisotropy

High resolution composite light microscope images of entire spurs were analyzed using custom MATLAB software to measure average cell length $\langle l(s) \rangle$ and cell width $\langle w(s) \rangle$ along the length of the spur, where s is the distance from the nectary tip in mm (Fig. SS4). The average cell anisotropy was then calculated as $\epsilon(s) = \frac{\langle l(s) \rangle}{\langle w(s) \rangle}$. In order to more clearly compare cell anisotropy for spurs of different instantaneous spur lengths L, we expressed the cell anisotropy $\epsilon(z)$ as a function of the scaled distance $z = s/L$. We note that this scaled distance z increases from $z = 0$ at the nectary tip to $z = 1$ at the attachment point, as shown in Fig. SS4.

(b) Spur radius profile

Digital photographs (Nikon D40x) of entire spurs were analyzed using custom MATLAB software to measure variation in spur radius along the length of the spur. The radius $r(s)$ (in mm) was determined using the appropriate scale bar for each image. To compare spur radius profiles between spurs of different instantaneous lengths L, we scaled both the radius r and the distance s by L. Defining $R = r/L$ and $z = s/L$, we compared scaled radial profiles $R(z)$ to illuminate differences in spur shape during development. As described in more detail in supplementary section M5 below, this scaled radial profile minimizes differences in overall size and highlights changes in spur shape.

M5. A SIMPLIFIED QUANTITATIVE MODEL OF SPUR DEVELOPMENT

During development, *Aquilegia* petal spurs both increase in overall size and change shape from a initial cup into a long, slender tube. Our microscope images of individual spur cells have demonstrated that each cell increases in size A and anisotropy ϵ throughout spur development. Our goal in modeling this process is to illuminate how these changes in size and shape at the cellular level determine morphological changes at the organ level.

As shown in Fig. 1 and Fig. SS1, the tubular shapes of developing *Aquilegia* petal spurs vary between species and are not perfectly conical. However, as shown in Fig $3F$ the radial profiles of *A. coerulea* are nearly linear. Therefore, a geometrically simple model spur shape can be used to provide intuition for the morphosis of actual spurs. In Fig. SS8A, we illustrate a simplified two dimensional model spur composed of initially square 'cells' with area A_0 and anisotropy $\epsilon_0 = 1$. The shape of any cylindrically symmetric spur can be mathematically described by a function $r(s)$, where r is the radius of the spur at a distance s from its tip. For the model spur depicted in Fig. SS8A, this radial function is linear: $r(s) = \frac{R_0}{L_0}s + H_0$, where R_0, H_0, and L_0 are the geometric parameters defined in Fig. SS8A. In order to explore how the combination of cell expansion and increased cell anisotropy affects the overall spur shape, in Fig. SS8B we depict the same spur following isotropic cell expansion by a factor $\alpha = A/A_0$ and increased cell anisotropy by a factor $\lambda = \epsilon/\epsilon_0$. Here A is the new cell area and ϵ is the new cell anisotropy. In this simplified model, all the cells change size and shape uniformly throughout the spur. The shape of the spur after this cell transformation is described by the radial profile

$$\begin{aligned} r(s) &= \frac{R}{L}s + H \\ &= \frac{1}{\lambda}\frac{R_0}{L_0}s + \sqrt{\frac{\alpha}{\lambda}}H_0, \end{aligned}$$

where $L = \sqrt{\alpha\lambda}L_0$, $R = \sqrt{\frac{\alpha}{\lambda}}R_0$, $H = \sqrt{\frac{\alpha}{\lambda}}H_0$, as shown in Fig. SS8$B$. We note that $r(s)$ depends on both the cell anisotropy factor λ and the cell expansion factor α. In order to eliminate the effect of overall isotropic expansion of the spur as a result of cell expansion, we define $R = r/L$ and $z = s/L$ and write the scaled radial profile $R(z)$ as

$$\begin{aligned} R(z) &= \frac{1}{\sqrt{\alpha\lambda}L_0}\left[\frac{1}{\lambda}\frac{R_0}{L_0}z\left(\sqrt{\alpha\lambda}L_0 + \sqrt{\frac{\alpha}{\lambda}}H_0\right)\right] \\ &= \frac{1}{\lambda}\left(\frac{R_0}{L_0}z + \frac{H_0}{L_0}\right). \end{aligned}$$

The function $R(z)$ does not depend on the cell expansion factor α, and thus it isolates the effect of increasing cell anisotropy on spur shape. Finally, it is possible to eliminate the effect on spur shape due to both cell expansion and increased cell anisotropy by defining $\tilde{R} = \lambda R$, for which the radial profile $\tilde{R}(z) = \left(\frac{R_0}{L_0}z + \frac{H_0}{L_0}\right)$ does not depend on α or λ.

During *Aquilegia* petal spur development, the cells both expand and become increasingly anisotropic; in the model spur this corresponds to a simultaneous increase in both α and λ. To illustrate such development, in Fig. SS9 we plot $r(s)$, $R(z)$, and $\tilde{R}(z)$ for a model spur with increasing values of α and λ. In Fig. SS9A, the $r(s)$ curves show

the unscaled radial profiles of the model spur throughout development from the initial red curve to the purple curve. These profiles are the result of the combined effects of increased cell anisotropy and cell expansion, and depict unscaled spur development. In Fig. SS9*B* the scaled $R(z)$ curves factor out isotropic expansion and isolate the anisotropic contribution to spur morphosis. In Fig. SS9*C*, where both expansion and anisotropic effects are canceled, the $\tilde{R}(z)$ curves collapse onto a single line.

Aquilegia petal spurs are not entirely linear, and our experiments have demonstrated that cell anisotropy ϵ varies along the length of the spur (Fig. 3). Nevertheless, the above description provides a useful framework for comparing the shapes of spurs with approximately linear radial profiles, such as *A. coerulea* and *A. longissima*. In Fig. SS10 we plot $r(s)$, $R(z)$, and $\tilde{R}(z)$ throughout spur development for both *A. coerulea* (Fig. SS10*A-C*) and *A. longissima* (Fig. SS10*D-F*). By comparing the $R(z)$ curves, which highlight the effect of cell anisotropy, it is clear that as cell anisotropy increases throughout development, the spur becomes more slender relative to its length (Fig. SS10*B* and *E*). In order to calculate $\tilde{R}(z)$ for both *A. coerulea* and *A. longissima* spurs, the value of λ must be determined at each developmental stage. Independent average ϵ measurements collected from cellular ESEM images as described in supplementary section M7 were used to calculate λ. The values of λ calculated from these independently measured cellular data result in collapsed radial profiles $\tilde{R}(z)$ (Fig. SS10*C* and *F*). The fact that the $\tilde{R}(z)$ curves in both Fig. SS10*C* and Fig. SS10*F* collapse onto a central shape indicates that the observed morphosis of the spurs is driven by the experimentally measured change in cell anisotropy ϵ for both species.

M6. NUMERICAL IMPLEMENTATIONS OF SPUR GROWTH

The simplified model of spur development described in the previous section overlooks the nonlinear spur shapes and nonuniform cell aspect ratio $\epsilon(z)$ in *Aquilegia* petal spurs. Despite this inaccuracy, the simplified model for spur morphosis still captures the essential trend of how cell expansion and anisotropy change spur shape throughout development, as shown by the scaled radius profiles in Fig. SS10*C* and *F*. A more precisely realistic model of spur development can be obtained by combining cellular level experimental data with tissue level radial profiles of young spurs.

As a starting point for numerical spur growth calculations, a generic 'initial' spur shape is determined by averaging two radial profiles from young *A. coerulea* spurs with length $L = 8$ mm. This averaged model spur profile was rotated around the long axis of the spur to create a cylindrically symmetric spur shape. Since our cellular measurements are binned into 13 points along the length of the spur at each developmental stage, we also binned the model spur into 13 points, and 'grew' each point according to available cellular measurements. Specifically, each of the 12 segments of the model profile was treated as approximately linear, with uniform cell anisotropy ϵ and cell area A. Within each segment, the framework of the simplified spur model described in the previous section was used to predict how each segment would develop. The i^{th} point (s_i, r_i) from the initial profile was mapped to its new position (s_i', r_i') according

to the relations

$$r'_i = \sqrt{\frac{\alpha_i}{\lambda_i}}\, r_i$$

$$s'_i = \begin{cases} 0 & i = 0 \\ s'_{i-1} + \sqrt{\alpha_i \lambda_i}\,(s_i - s_{i-1}) & i > 0 \end{cases}$$

where ϵ_i and α_i are taken from cellular measurements corresponding to the position of point i at the developmental stage of interest. The resulting numerically calculated profiles (s', r') (plotted in Fig. $3F$) were finally rotated about the long axis of the spur to create the three dimensional spurs depicted in Fig. $3F$. In stark contrast to these spurs, the numerical spurs shown in Fig. SS11 were calculated using only cell area data, ignoring the effect of cell anisotropy. Clearly these numerically calculated spurs do not accurately capture the shapes of developing *A. coerulea* spurs.

M7. TREATMENT OF *Aquilegia* SPURS WITH ORYZALIN

Oryzalin was suspended in lanolin at a concentration of ∼10 µM and applied topically to developing spurs. Exploiting the fact that all *Aquilegia* species have five petals per flower, one petal was treated, while the remaining four petals were used as controls.

M8. ENVIRONMENTAL SCANNING ELECTRON MICROSCOPY (ESEM) METHODS

ESEM images were collected using Zeiss-EVO Environmental Scanning Electron Microscope (Harvard University, Center for Nanoscale Science). *Aquilegia* petal spurs are very fragile and collapse upon dehydration, rendering high-vacuum SEM impossible. Thus, ESEM was performed at low vacuum (∼ 10 Pa) which allowed for immediate wet imaging of untreated and undamaged samples. This technique also allowed for higher throughput since time consuming high vacuum tissue preparation methods could be avoided.

ESEM images of spur cells were collected from *A. vulgaris*, *A. canadensis*, *A. coerulea*, and *A. longissima*. ESEM images were taken at four points along the axis of the petal (Fig. SS14). Data for seven petal lengths were collected for *A. coerulea*, four petal lengths for *A. vulgaris*, four petal lengths for *A. longissima*, and four petal lengths for *A. canadensis*. Two to four biological replicates were imaged for each of the four points along the spur at each petal length for a total of ∼ 228 distinct mean cell measurements. Cellular morphological data was collected from the ESEM images using ImageJ EllipseFitter (http://rsbweb.nih.gov/ij/).

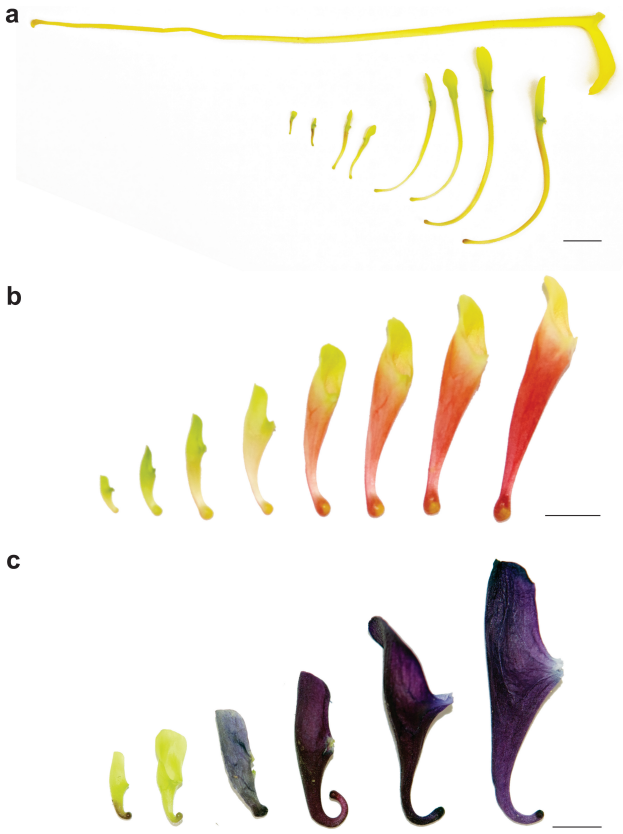

FIG. S1: **Developmental series of *Aquilegia* petals.** (*a*) *A. longissima*. (*b*) *A. canadensis*. (*c*) *A. vulgaris*. All scale bars equal 1 cm.

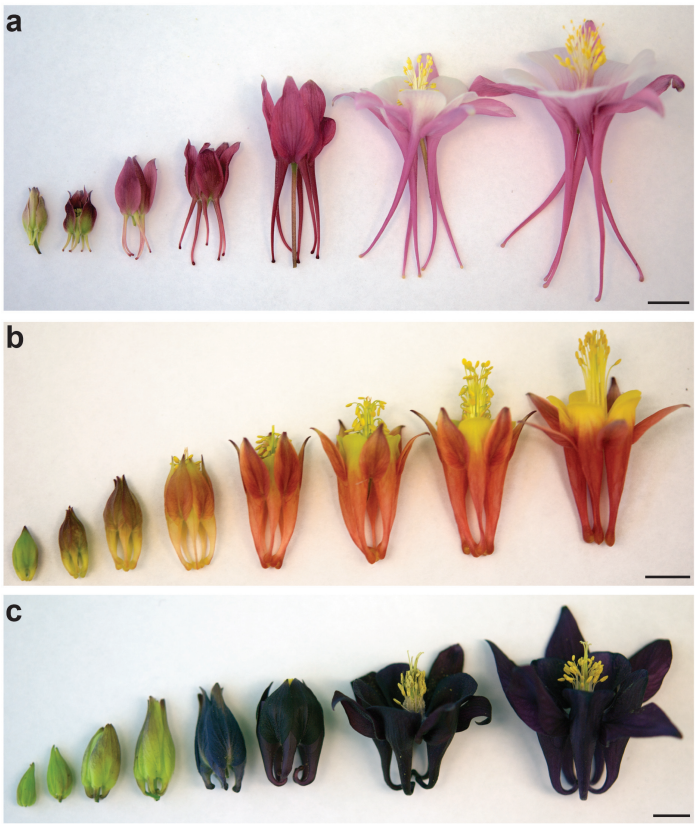

FIG. S2: **Developmental series of *Aquilegia* flowers.** (*a*) *A. coerulea* 'Origami' red/white. (*b*) *A. canadensis*. (*c*) *A. vulgaris*. All scale bars equal 1 cm.

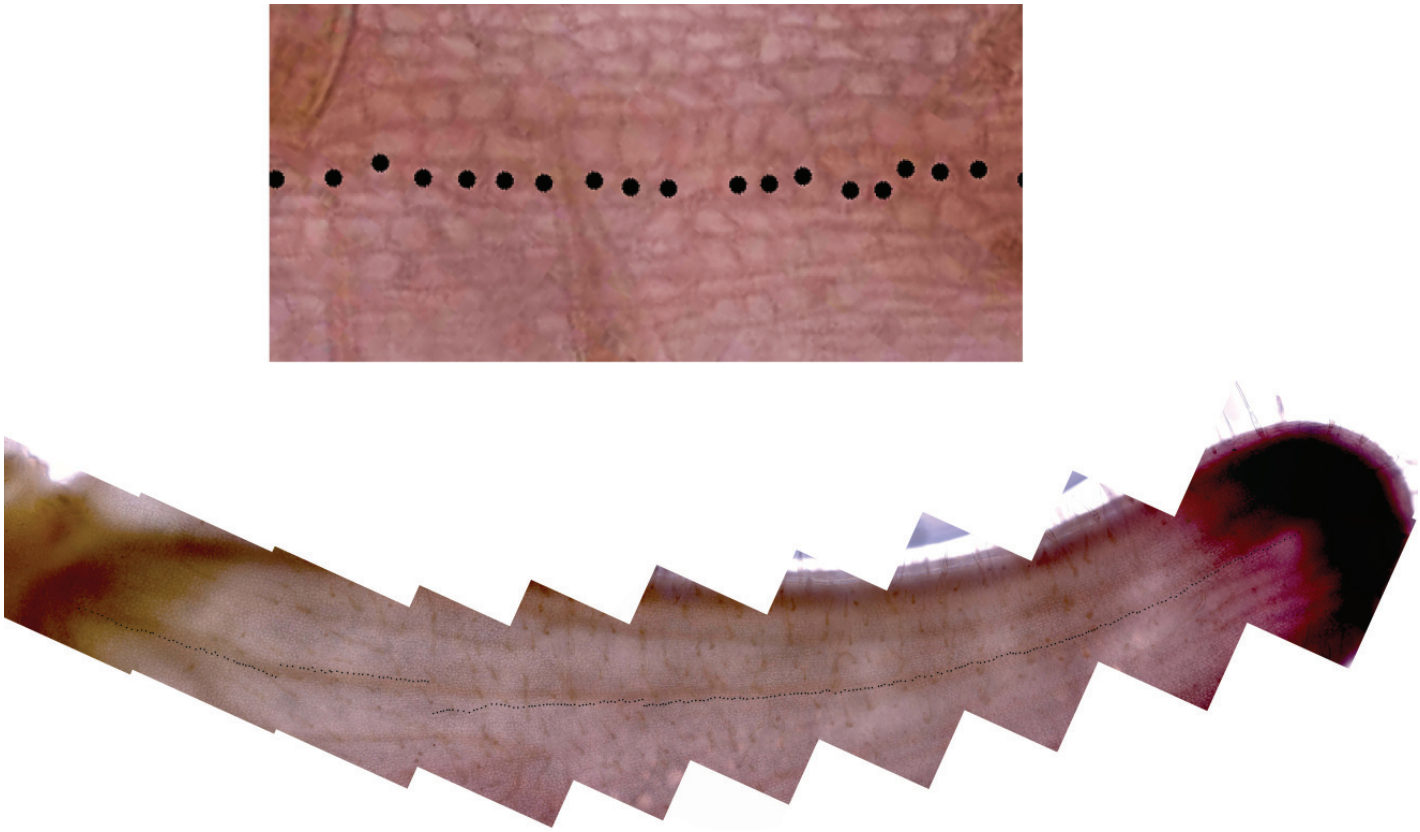

FIG. S3: **Direct measurement of cell number during development.** Typical cellular resolution image shown with overlaid dots indicating manually counted cells.

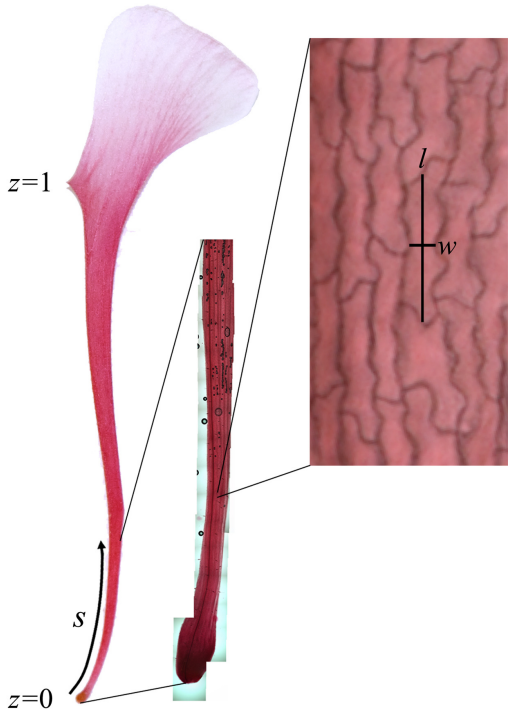

FIG. S4: **Typical composite microscope image of a spur, used for measuring cell morphology along the length of the spur.** Custom MATLAB software was used to measure the length $l(s)$ and width $w(s)$ of cells throughout the spur. The average length and width at a distance s (in mm) from the nectary tip was then used to calculate the average cell anisotropy $\epsilon(s)$ and area $A(s)$. Left, image of entire petal. Center, composite microscope image of lower portion of spur. Right, full magnification microscope image showing cellular resolution.

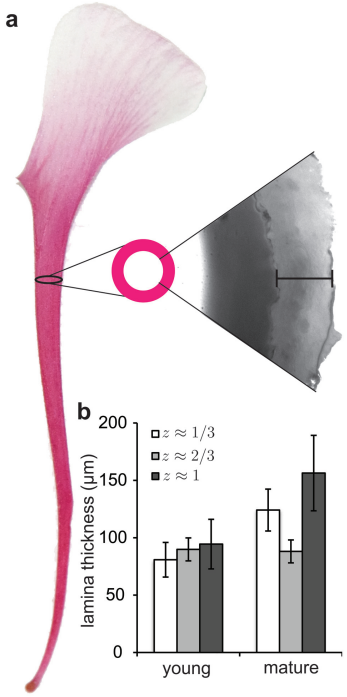

FIG. S5: **Spur lamina thickness measurements.** (a) Cross sections of spurs viewed under light microscopy to measure lamina thickness. (b) Lamina thickness does not vary significantly with z in young and mature spurs.

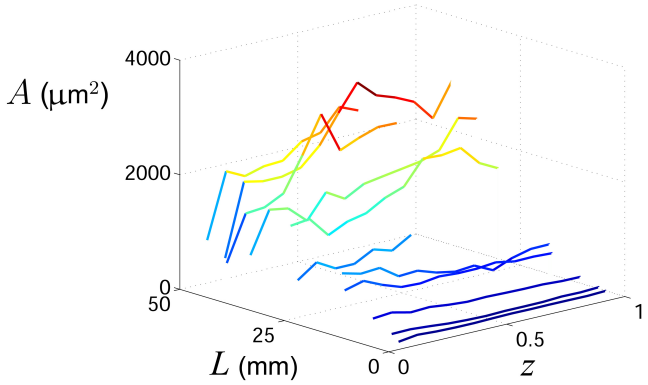

FIG. S6: **Cell area along the length of the spur throughout development.** Unlike cell anisotropy, cell area increase is virtually uniform throughout the spur during spur elongation.

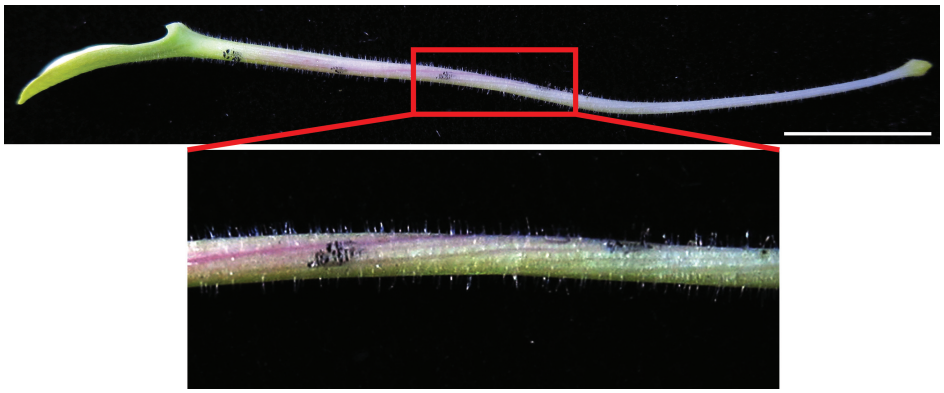

FIG. S7: ***A. longissima* spur with twisted cell files.** Black smudges are ink marks added to aide measurement of twisting during growth. Scale bar equals 1cm.

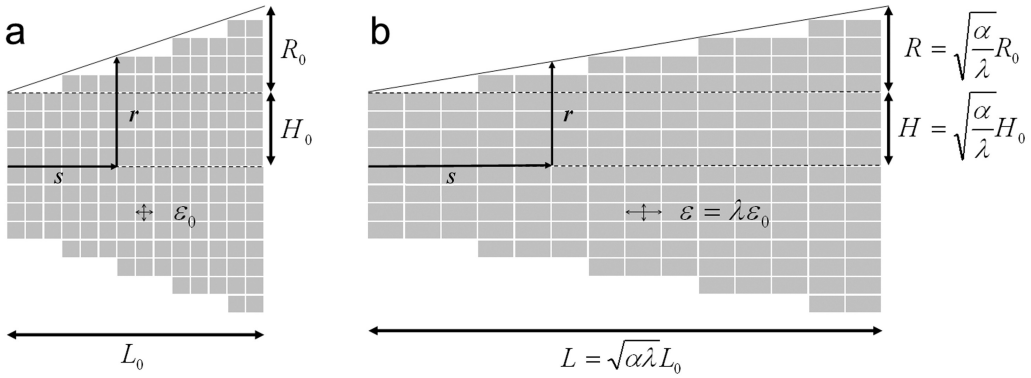

FIG. S8: **Illustration of a simplified two dimensional trapezoidal model of a spur.** (a) The initial spur shape is described by the radius function $r(s) = \frac{R_0}{L_0} s + H_0$. (b) Following both uniform cell expansion by a factor α and an increase in cell anisotropy by a factor λ, the spur takes on a new shape described by $r(s) = \frac{R}{L} s + H$.

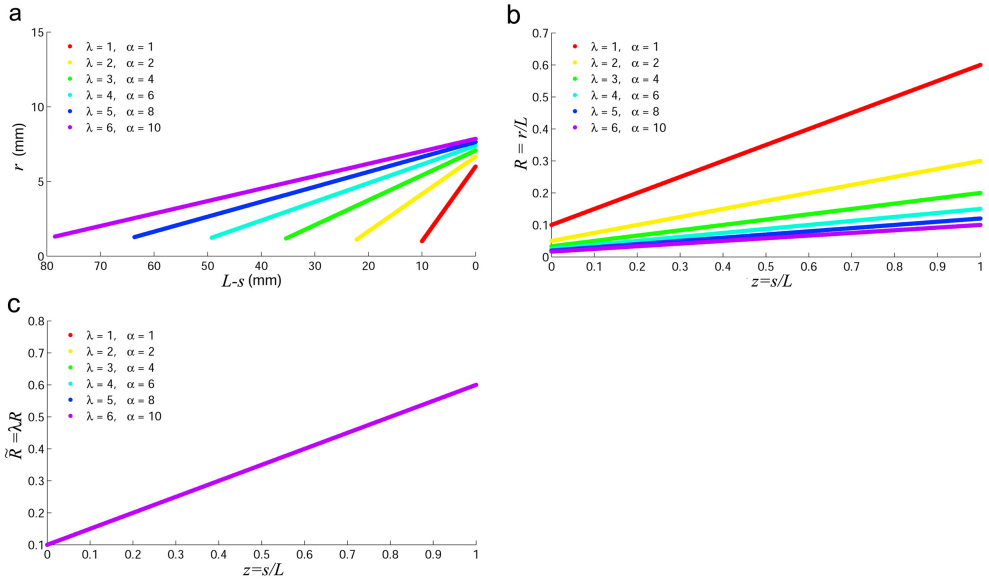

FIG. S9: **Radius functions for a model spur as α and λ are increased to mimic spur development.** The initial spur parameters R_0, H_0, and L_0 remain constant throughout development. (a) The unscaled radius function $r(s)$ shows the change in both size and shape of the model spur from its initial shape (red curve) to its final shape (purple curve). (b) The scaled radius function $R(z)$ isolates the effect of cell anisotropy. (c) The fully scaled radius function $\tilde{R}(z)$ eliminates the effects of both isotropic cell expansion and increased cell anisotropy.

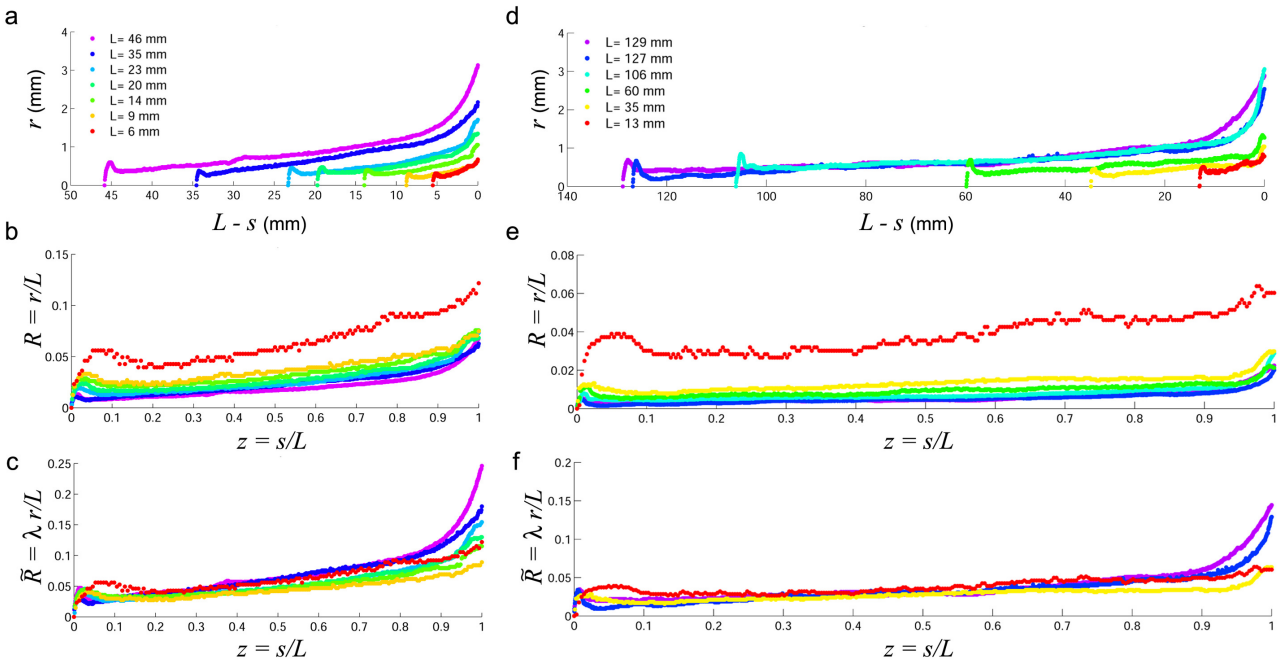

FIG. S10: ***Aquilegia* spur radial profiles $r(s)$, $R(z)$, and $\tilde{R}(z)$ throughout development.** (a - c), *A. coerulea*. (d - f), *A. longissima*. The values of λ used to calculate $\tilde{R}(z)$ are determined from independent ESEM measurements of cell anisotropy. Definitions of $r(s)$, $R(z)$, and $\tilde{R}(z)$ are provided in the text.

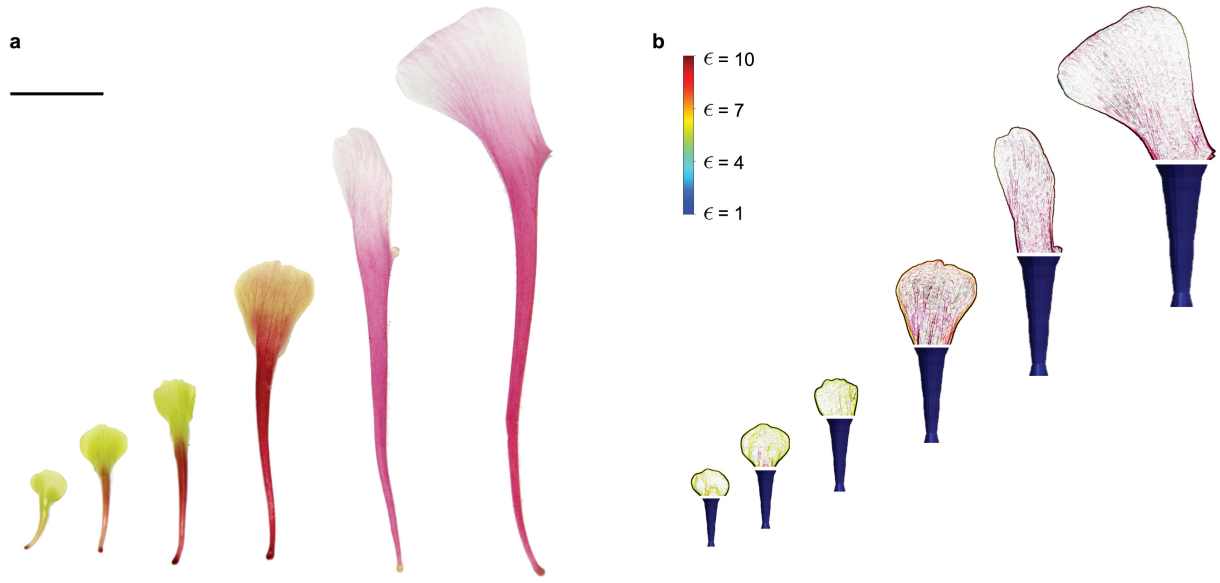

FIG. S11: **Numerically calculated spurs omitting the effect of cell anisotropy have the wrong shape.** (a) Developmental series of *A. coerulea* petals. Scale bar equals 1 cm. (b) Using cell area measurements while ignoring cell anisotropy measurements, the same shortest numerical spur shown in Fig. 2e is grown to each of the developmental stages shown in panel (a).

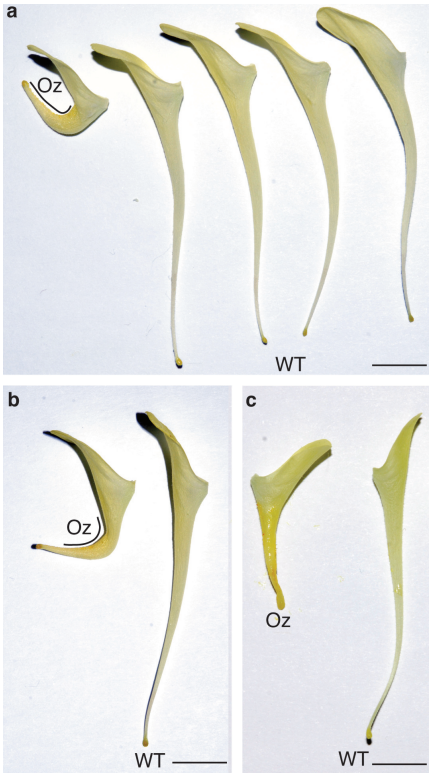

FIG. S12: **Oryzalin treatment of *Aquilegia chrysantha* petals.** Oz, oryzalin. All spurs were treated at spur length $L \approx 1$ cm corresponding to an early developmental stage. Untreated petals from the corresponding flower are shown as controls. Photos of petals were taken ~ 6 days after initial application of oryzalin. (a - b) Oryzalin was applied in one strip (as indicated by the line) on the developing spur. Inhibiting cell anisotropy via oryzalin on one side of the spur, while the cells on the opposite side continue to elongate, results in a curved spur. All four untreated petals are shown alongside oryzalin treated petal in panel (a). (c) Oryzalin was applied on the entire surface of the developing *Aquilegia* spur. All scale bars equal 1 cm.

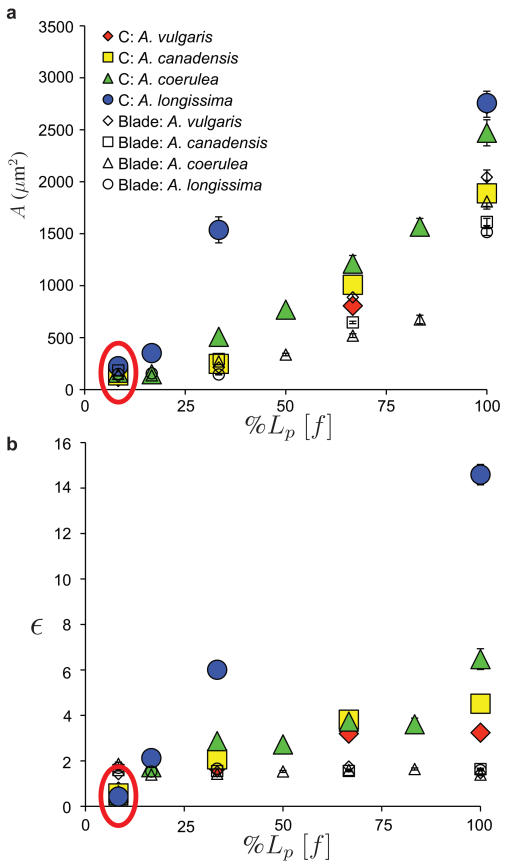

FIG. S13: **Cell area A and cell anisotropy ϵ measured at position C on the spur and at position Blade on the petal blade, for four *Aquilegia* species.** Cell data was collected from ESEM images taken at multiple developmental stages for each species, for a total of $\sim$ 6500 cell measurements. (a) Cell area A is plotted against percent final petal length $L_p[f]$ for each species at both petal positions, C and Blade. Cell area increases uniformly along the entire length of the petal for all species. (b) Cell anisotropy ϵ is plotted against percent final petal length $L_p[f]$ for each species. Cell anisotropy remains constant in the petal blade for all species, while in the spur cell anisotropy increases more dramatically in species with longer spurs.

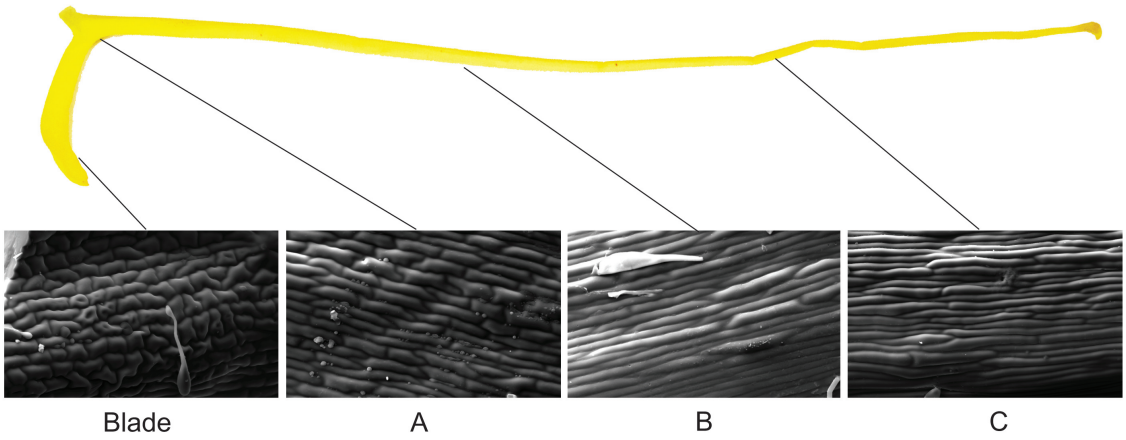

FIG. S14: **Relative location of data collection points Blade, A, B, and C.** Representative ESEM images from each location are shown below.